J18.1 QUANTITATIVE PROBABILISTIC MODEL FOR URBAN DISPERSION

Eugene Yee[1]* and Bing-Chen Wang[2]

[1]Defence R&D Canada – Suffield, P.O. Box 4000, Medicine Hat, AB, T1A 8K6, Canada

[2]Department of Mechanical and Manufacturing Engineering, University of Manitoba, Winnipeg, Manitoba, R3T 5V6, Canada

God is not so cruel as to create situations described by nonlinear differential equations.

— Edward Sexton

1. INTRODUCTION

There are, quite rightly, growing concerns worldwide about the dangers, both actual and potential, resulting from the atmospheric release (either accidental or deliberate) of hazardous materials. This concern is particularly acute in densely populated urban areas. In addition, there is the spectre that terrorist organizations could potentially release hazardous chemical, biological, radiological, or nuclear (CBRN) materials in a city. As a consequence, governments and their agencies, sometimes acting multinationally, are supporting the development of methodologies to counter and/or to mitigate the consequences resulting from the release of noxious substances into the urban environment. The development of such methodologies would be greatly facilitated by mathematical modeling.

In the case of hazardous material releases in a built-up environment, effective mitigation in these settings will require an understanding of the turbulent transport and diffusion of these contaminants in an urban environment. Over the past decade, considerable effort has been expended from the experimental, empirical, and theoretical points of view to understand the flow and dispersion in the urban environment on a wide range of scales from the very large (at the regional and city scales) to the quite small (at the neighborhood and street, even building, scales).

Modeling the transport and dispersion of pollutants in the urban area has been the subject of much recent effort. Hall et al. (1997) describe an empirical Gaussian puff model that considers the local interaction of puffs with obstacles. A semi-empirical urban diagnostic wind model (QUIC-URB)[1], which is used to provide the necessary velocity statistics for a Lagrangian stochastic model of urban dispersion (QUIC-PLUME), has been described by Williams et al. (2004). Computational fluid dynamics (CFD) has recently been applied to the modeling of urban dispersion. There are essentially two different approaches to the numerical modeling of dispersion through an urban area using CFD; namely, the Reynolds-averaged Navier-Stokes (RANS) and large-eddy simulation (LES) approaches. The application of CFD to turbulent dispersion in the urban environment using either RANS or LES include Liu and Barth (2002), Baik et al. (2003), Kim and Baik (2004), Camelli et al. (2005), Coirier et al. (2005), Hsieh et al. (2007) and Milliez and Carissimo (2007). A hybrid approach, which uses a RANS-predicted gridded field of (building-resolving) wind statistics in an urban area as input to a three-dimensional Lagrangian stochastic trajectory model for the prediction of urban dispersion, is described by Wilson (2007).

The modeling of the dispersion of hazardous materials in urban areas has focussed primarily on the prediction of the ensemble-averaged distribution of material (or, mean concentration) from a source. Unfortunately, for many practical applications, it is necessary to estimate both the mean and fluctuating values of concentration (the latter of which can be characterised by moments of concentration of second order and higher). For example, the statistical properties of concentration fluctuations in a dispersing plume are important to the assessment of risk from the release of certain highly toxic materials (e.g., industrial chemicals, chemical warfare agents) in which there is a nonlinear relationship between concentration and duration of exposure for a given level of harmful effect. Similarly, short-term concentration fluctuations are very relevant to estimating ignition hazard from the leakage of flammable gases (e.g., fuel-air mixtures, liquefied natural gas spills) in which it is necessary to determine the probability that the instantaneous concentration lies between the lower and upper flammability limits. Still other important applications include the prediction of the probability of visibility through obscurant clouds and the characterization of the perception of odours required to evaluate the nuisance due to malodourous substances.

The development of urban dispersion models for the higher-order moments of concentration has been hampered by the lack of comprehensive data sets involving measurements of the behavior of concentration fluctuations in plumes dispersing in an urban area. It is only relatively recently that experiments, providing detailed measurements of concentration fluctuations in clouds and plumes dispersing through a built-up environment, have begun to appear. For example, Yee and Biltoft (2004) describe a series of tracer experiments studying the statistical properties of concentration fluctuations (e.g., concentration variance, concentration probability density function, various concentration time and length scales of dominant plume motions) in a plume dispersing through a large array of building-like obstacles (an experiment referred to as the Mock Urban Setting Test, or MUST). Gailis and Hill (2006) report a wide range of concentration statistics and other quantitative descriptors of plume behaviour for tracer dispersion in a boundary-layer wind-tunnel simulation of the MUST experiment. Yee et al. (2006) provided detailed comparisons

* *Corresponding author address*: Hazard Protection Section, Defence R&D Canada – Suffield, P.O. Box 4000, Medicine Hat, AB, T1A 8K6, Canada, e-mail:eugene.yee@drdc-rddc.gc.ca

[1] QUIC is an acronym for Quick Urban and Industrial Complex.

of concentration statistics in a plume dispersing through the MUST obstacle array at three different scales; namely, at full-scale in a field experiment, at 1:50 scale in a wind-tunnel simulation, and at 1:205 scale in a water-channel simulation. Finally, Klein et al. (2008) analyzed and compared concentration fluctuation measurements from the Joint Urban 2003 full-scale and wind-tunnel experiments.

With the availability of measurements of concentration fluctuations in a plume dispersing in an urban area, efforts to model the concentration variance (second-order moment of concentration) for urban plumes have been undertaken recently (e.g., Andronopoulos et al., 2002; Hsieh et al., 2007; Wang et al., 2007; Wang et al., 2008; and, Milliez and Carissimo, 2008). Following from this earlier work, the objective of this paper is to develop a full probabilistic model for concentration fluctuations in contaminant clouds or plumes, which can be used to assess actual or potential hazards associated with releases of harmful materials in urban areas. A preliminary description of this probabilistic model for urban dispersion will be described herein, but a more complete exposition is available in Yee et al. (2009).

2. MODEL FORMULATION

2.1 Overview

The main components of our probabilistic model for urban dispersion are exhibited in Fig. 1. There are three components in the modeling schemata. The first component is the urban flow component. This component uses Reynolds-averaged Navier-Stokes (RANS) methodology, with a two-equation k-ϵ turbulence closure model, to predict the complex and highly disturbed wind flows in an urban area. This mean flow and turbulence model provides the spatially-varying velocity (wind) statistics of the urban flow required by the second component, which is the urban dispersion component. This component consists of the turbulent-transport model for the concentration fluctuations, which involves the solution of the transport equations for the mean concentration C and concentration variance $\overline{c'^2}$. The third component involves the specification of a functional form for the concentration probability density function (PDF). To this purpose, the two lowest-order moments of concentration (viz., mean concentration and concentration variance) obtained in the second component are used to determine the parameters for the concentration PDF, whose form (clipped-gamma distribution) has been prespecified. Now, we proceed to describe each one of these model components.

2.2 Urban flow component

The RANS approach is used to predict the strongly-disturbed wind statistics (e.g., mean wind and turbulence quantities) associated with the complex flow through and above an urban area, consisting of the arbitrary groupings of buildings in various configurations that are characteristic of a real cityscape. In this approach, each of the velocity components is separated into two parts: a mean value and a turbulent portion. Next, the Reynolds method consists of averaging each of the equations of motion and the continuity equation. Closure of these equations is obtained using a two-equation k-ϵ turbulence model. This results in a system of nonlinear partial differential equations governing mass and mean momentum conservation which can be expressed in Cartesian coordinates as follows (assuming an incompressible and adiabatic fluid):

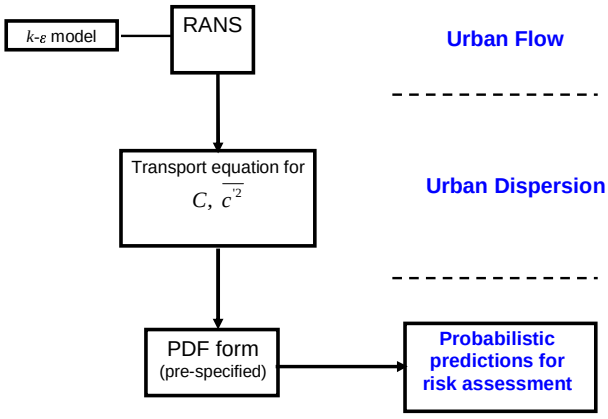

Figure 1: Main components of probabilistic model for urban dispersion.

Continuity:

$$\frac{\partial \bar{u}_i}{\partial x_i} = 0; \tag{1}$$

Mean Momentum:

$$\frac{\partial \bar{u}_i}{\partial t} + \frac{\partial \bar{u}_j \bar{u}_i}{\partial x_j} = -\frac{\partial \bar{p}}{\partial x_i} + \nu \frac{\partial^2 \bar{u}_i}{\partial x_j^2} - \frac{\partial}{\partial x_j}(\overline{u_i' u_j'}); \tag{2}$$

Kinematic Eddy Viscosity:

$$\nu_t = C_\mu k^2/\epsilon; \tag{3}$$

Turbulence Kinetic Energy:

$$\frac{\partial k}{\partial t} + \frac{\partial \bar{u}_j k}{\partial x_j} = \frac{\partial}{\partial x_j}\left[\left(\nu + \frac{\nu_t}{\sigma_k}\right)\frac{\partial k}{\partial x_j}\right] + P_k - C_{\epsilon 0}\epsilon; \tag{4}$$

Viscous Dissipation Rate:

$$\frac{\partial \epsilon}{\partial t} + \frac{\partial \bar{u}_j \epsilon}{\partial x_j} = \frac{\partial}{\partial x_j}\left[\left(\nu + \frac{\nu_t}{\sigma_\epsilon}\right)\frac{\partial \epsilon}{\partial x_j}\right] + \frac{\epsilon}{k}(C_{\epsilon 1} P_k - C_{\epsilon 2}\epsilon); \tag{5}$$

Closure Coefficients:

$$C_{\epsilon 1} = 1.44, \quad C_{\epsilon 2} = 1.92, \quad C_\mu = 0.09, \quad \sigma_k = 1.0. \tag{6}$$

In Eqs. (1) to (6), a bar over the quantity is used to denote Reynolds averaging. The Einstein summation convention is used, which prescribes that if any of the indices is repeated in a term, a summation over that index is implied. Here, $\bar{u}_i$ and u_i' are the mean and fluctuating velocities in the x_i-direction, respectively, with the subscript $i = 1$, 2, or 3 representing the streamwise x, cross-stream y, or vertical z directions; $x_i = (x, y, z) \equiv \mathbf{x}$; t is time; $u_i = (u, v, w)$; $\bar{u}_i = (\bar{u}, \bar{v}, \bar{w})$;[2] ν is the kinematic viscosity and $\bar{p}$ is the kinematic mean pressure (with p' used to denote pressure fluctuations).

The tensor $\overline{u_i' u_j'}$ appearing in the transport equation for the mean momentum is the kinematic Reynolds stress tensor,

[2] with the implied Reynolds decomposition $u_i = \bar{u}_i + u_i'$.

which is modeled here using the Boussinesq eddy-viscosity approximation which links the Reynolds stresses to the mean rates of strain (deformation) as follows:

$$\overline{u_i' u_j'} = \frac{2}{3} k \delta_{ij} - \nu_t \left(\frac{\partial \bar{u}_i}{\partial x_j} + \frac{\partial \bar{u}_j}{\partial x_i} \right), \tag{7}$$

where ν_t is the kinematic eddy viscosity, $k \equiv \frac{1}{2}\overline{u_i' u_i'}$ is the turbulence kinetic energy (TKE), and δ_{ij} is the Kronecker delta function. In Eq. (4) (transport equation for TKE), the term P_k is the production of k defined as

$$P_k \equiv -\overline{u_i' u_j'} \frac{\partial \bar{u}_i}{\partial x_j}. \tag{8}$$

Finally, ϵ is the viscous dissipation of TKE whose transport equation is given by Eq. (5).

Equation (4) represents the standard transport equation for TKE, except that an additional coefficient C_{ϵ_0} has been incorporated in this transport equation to adjust the balance between the production and dissipation of TKE. If $C_{\epsilon_0} = 1$, the transport equation for TKE reduces to the standard form. The coefficient C_{ϵ_0} was introduced because it can be demonstrated (see later) that a non-unity value for C_{ϵ_0} can provide improved predictions of the turbulence energy levels in obstacle arrays[3] (especially those that exhibit skimming flow over the buildings, with a concomitant limited penetration of the flow aloft into the spaces between the buildings). The k-ϵ model with $C_{\epsilon_0} \neq 1$ will be referred to henceforth as the modified k-ϵ model. When $C_{\epsilon_0} = 1$, the modified k-ϵ model reduces to the standard k-ϵ model.

A closed-form solution for the modified k-ϵ model can be obtained for the neutral wall shear layer. The solution gives

$$\bar{u} = \frac{u_*}{k_v} \log z + B, \qquad k = \frac{u_*^2}{\sqrt{C_\mu}}, \qquad \epsilon = \frac{u_*^3}{k_v z}, \tag{9}$$

where $u_* \equiv \left(-\overline{u'w'}\right)^{1/2}$ is the friction velocity and B is a constant of integration. For this analytical solution, we find an implied value for the von Kármán constant, k_v, of

$$k_v^2 = C_\mu^{1/2} \left(C_{\epsilon 2} - C_{\epsilon 1} C_{\epsilon_0} \right) \sigma_\epsilon / C_{\epsilon_0}. \tag{10}$$

It should be noted that for the standard k-ϵ model, $C_{\epsilon_0} = 1$. Using the closure coefficient values for the standard k-ϵ model [cf. Eq. (6) and with $\sigma_\epsilon = 1.3$], k_v assumes a value of 0.43. The experimental values for k_v are primarily in the range 0.41 ± 0.2, so the implied value of k_v in the k-ϵ model is consistent with these measurements. For the case where $C_{\epsilon_0} \neq 1$ (modified k-ϵ model), the coefficient σ_ϵ is assigned the value $\sigma_\epsilon = k_v^2 C_{\epsilon 0} / [C_\mu^{1/2} (C_{\epsilon 2} - C_{\epsilon 1} C_{\epsilon 0})]$ in order to be consistent with the compatibility condition for flow in a wall shear layer, given by Eq. (10).[4] For the modified k-ϵ model, we will use $C_{\epsilon 0} = 0.7$. This value for $C_{\epsilon 0}$ has been shown by Wang et al. (2007) to provide improved predictions of turbulence energy levels in obstacle arrays, in comparison to those provided by the standard k-ϵ model.

[3] Previous investigations such as Lien and Yee (2004) and Coirier et al. (2005) have demonstrated that the standard k-ϵ turbulence closure scheme (and its variants such as Kato-Launder and renormalized group (RNG) forms) has a tendency to underpredict the turbulence energy levels in obstacle arrays.

[4] Naturally, with $C_{\epsilon 0} = 1$, the closure coefficient $\sigma_\epsilon = 1.3$ which is the conventional value used in the standard k-ϵ model.

2.3 Urban dispersion component

The wind statistics of the highly disturbed flow in the urban environment are available from the urban flow component. This information can be used to "drive" an urban dispersion model to predict the transport and diffusion of pollutants (contaminants) released in the urban area. The transport equation for the mean concentration C of the pollutant has the following form:

Mean concentration:

$$\frac{\partial C}{\partial t} + \frac{\partial \bar{u}_j C}{\partial x_j} = \frac{\partial}{\partial x_j} \left[\left(D \delta_{jk} + D_{jk}^t \right) \frac{\partial C}{\partial x_k} \right] + Q, \tag{11}$$

where D is the molecular kinematic diffusivity of the pollutant in air and Q is the source density distribution for the contaminant. The transport equation for C has the form of an advection-diffusion equation, and implicit in this form is the application of the generalized gradient diffusion hypothesis to model the turbulent concentration fluxes; namely,

$$\overline{u_j' c'} = -D_{jk}^t \frac{\partial C}{\partial x_k}, \tag{12}$$

where the tensor eddy diffusivity D_{jk}^t is defined as

$$D_{jk}^t = C_{s1} \frac{k^2}{\epsilon} \delta_{jk} + C_{s2} \frac{k^3}{\epsilon^2} \left(\frac{\partial \bar{u}_j}{\partial x_k} + \frac{\partial \bar{u}_k}{\partial x_j} \right). \tag{13}$$

Here, $C_{s1} = 0.134$ and $C_{s2} = -0.032$ are two model coefficients (Yoshizawa, 1985).

In addition to the prediction of the mean concentration C, we predict also the concentration variance $\overline{c'^2}$ using its transport equation. The transport equation for $\overline{c'^2}$ has the following form:

Concentration variance:

$$\frac{\partial \overline{c'^2}}{\partial t} + \frac{\partial (\bar{u}_j \overline{c'^2})}{\partial x_j} = \frac{\partial}{\partial x_j} \left(D \frac{\partial \overline{c'^2}}{\partial x_j} - \overline{u_j' c'^2} \right) - 2 \overline{u_j' c'} \frac{\partial C}{\partial x_j} - \epsilon_c, \tag{14}$$

where ϵ_c is the molecular dissipation of $\overline{c'^2}$. As in the case of the transport equation for the mean concentration, the turbulent flux of $\overline{c'^2}$ is modeled using a tensor eddy diffusivity model as follows:

$$\overline{u_j' c'^2} = -D_{jk}^t \frac{\partial \overline{c'^2}}{\partial x_k}, \tag{15}$$

where D_{jk}^t is determined in accordance to Eq. (13). The implicit assumption used here is that the concentration variance diffuses in exactly the same manner as the mean concentration.

The critical term that requires modeling in the transport equation of $\overline{c'^2}$ is the scalar dissipation ϵ_c. The modeling of this term determines effectively the rate at which concentration fluctuations in the dispersing plume are destroyed by the molecular diffusion. The scalar dissipation ϵ_c can be modeled algebraically as $\epsilon_c = \overline{c'^2}/t_d$, where t_d is the dissipation time scale that is related to the characteristic decay time of concentration fluctuations in the plume. To complete the model, we need a parameterization for t_d. The difficulty in modeling t_d

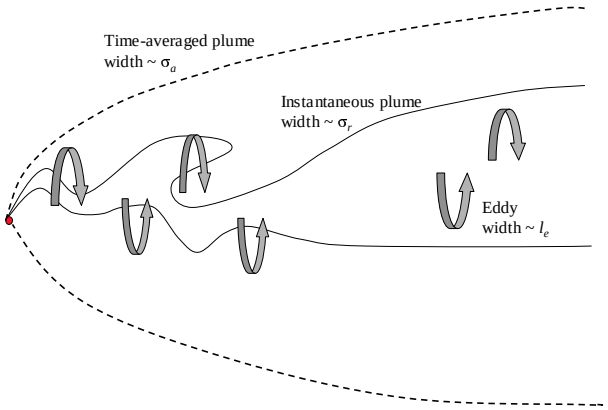

Figure 2: Schematic diagram of fluctuating plume illustrating the effect of the eddy size spectrum in the determination of the inner and outer scales of plume motion that define the internal (in-plume mixing) and external (plume meander) concentration fluctuations.

arises from the fact that it is necessary to distinguish between the temporal scales responsible for the plume meander (external fluctuations) and those responsible for the in-plume mixing (internal fluctuations), because it is only the latter time scales that are associated with scalar dissipation. The external fluctuations arising from plume meander are non-dissipative and do not contribute to the "destruction" of the concentration variance.

Figure 2 provides a highly-simplified cartoon depicting the spatial development of a plume from a compact (localized) source within the framework of a fluctuating plume model (Yee et al., 1994; Yee and Wilson, 2000). Turbulent eddies (blobs or lumps of vorticity) with a wide spectrum of scales (spanning the range from the Kolmogorov microscale Λ_K to the integral scale of turbulence Λ_I) exist in the atmosphere. Consider the action of eddies of length scale l_e on the plume. At a given stage in the spatial development of the plume (or, equivalently, at a fixed downwind distance from the localized source), turbulent eddies of size $l_e \gg \sigma_r$ (σ_r is the width of the instantaneous plume) result in the bulk meandering of the instantaneous plume. Eddies with size $l_e \approx \sigma_r$ cause distortion of the instantaneous plume boundary as clean air packets are entrained into the body of the plume, resulting in the growth of σ_r. Hence, σ_r corresponds to an inner plume length scale of turbulent diffusion associated with internal fluctuations. In view of this, the dissipation time scale t_d is intimately related to the time scales associated with the internal plume fluctuations, as it is the destruction of these fluctuations that determines the scalar dissipation.

As eddies of size $l_e \approx \sigma_r$ "break up", they result in turbulent stirring (or, strain-induced stretching) of the plume material lines which, in turn, enhances molecular mixing (or, molecular diffusion of the plume material across the intermaterial surfaces). The dissipation time t_d is associated with the break-up time of these eddies. For a turbulent eddy of size $l_e = \sigma_r$ (with $l_e < \Lambda_I$) and characteristic velocity scale $\Delta v(l_e)$, the rate for turbulence energy to cascade down to smaller scales is $\Pi_{l_e} \sim \epsilon \sim (\Delta v(l_e))^2/(l_e/\Delta v(l_e)) = (\Delta v(l_e))^3/l_e$ since an eddy breaks up on a time scale of its turn-over time. Consequently, $\Delta v(l_e) \sim (\epsilon l_e)^{1/3}$. At the scale corresponding to the integral length scale of turbulence with $l_e = \Lambda_I$, one expects that $\Delta v(\Lambda_I) \sim (\epsilon \Lambda_I)^{1/3} = k^{1/2}$ so $\Delta v(l_e)/\Delta v(\Lambda_I) = (l_e/\Lambda_I)^{1/3}$ implying

$$\Delta v(l_e) = k^{1/2} \left(\frac{l_e}{\Lambda_I}\right)^{1/3}, \qquad l_e = \sigma_r \ll \Lambda_I. \tag{16}$$

For an inner plume scale σ_r ($\sigma_r < \Lambda_I$), the average rate of increase of σ_r should depend only on $\Delta v(l_e)$ with $l_e = \sigma_r$ because only turbulent eddies of size l_e (eddies of size comparable to the instantaneous plume width) contribute to the growth of the instantaneous plume (see Fig. 2), so

$$\frac{dl_e}{dt} \sim \Delta v(l_e) \sim (\epsilon l_e)^{1/3}, \qquad l_e = \sigma_r \ll \Lambda_I, \tag{17}$$

where the temporal rate of increase in Eq. (17) is used to denote the spatial development of the plume, to be interpreted in the sense that the time t should be synonymous with $x/\mathcal{U}_p$ where $\mathcal{U}_p$ is the transport speed for the plume dispersion. Integration of Eq. (17) gives $l_e \sim \epsilon^{1/2} t^{3/2}$ or, equivalently, on introducing explicitly the constant of proportionality in this relationship:

$$l_e^2(t) - l_e^2(0) = C_r \epsilon t^3, \qquad t \geq 0, \tag{18}$$

which can be recognized as the Richardson-Obukhov 4/3-law for plume growth in the relative diffusion framework (recalling that as the plume width σ_r increases with t, only those eddies with size $l_e \approx \sigma_r$ contribute to its growth). The constant C_r in Eq. (18) can be identified as Richardson-Obukhov constant, which we take to have the value 0.55. Finally, we associate $l_e(0)$ in Eq. (18) with the initial (finite) size σ_0 of the source.

In the regime of plume development where $\sigma_0 \leq \underline{l_e} \equiv \sigma_r \ll \Lambda_I$, the scalar dissipation can be modeled as $\epsilon_c = \overline{c'^2}/t_d$, with the dissipation time scale $t_d \propto l_e/\Delta v(l_e)$, where the dissipation length scale l_e and velocity scale $\Delta v(l_e)$ are determined in accordance to Eqs. (16) and (18), respectively. There is an explicit association of $t_d(t)$ at travel time t, with the eddy break-up time (assumed to be comparable to the eddy turnover time) for eddies of size $l_e \approx \sigma_r(t)$. More specifically,

$$\begin{aligned} t_d \propto l_e/\Delta v(l_e) &= \frac{k}{\epsilon}\left(\frac{l_e}{\Lambda_I}\right)^{2/3} \\ &= t_I \left(\frac{l_e}{\Lambda_I}\right)^{2/3}, \qquad l_e \ll \Lambda_I, \end{aligned} \tag{19}$$

where $t_I \equiv k/\epsilon$ is the integral turbulence time scale. Eq. (19) implies that $t_d \propto t$ for the regime of plume development where $\sigma_r \ll \Lambda_I$.

Once the instantaneous plume width $l_e = \sigma_r$ exceeds the integral turbulence scale Λ_I, the Richardson-Obukhov 4/3-law fails owing to the fact that there are no eddies larger than Λ_I. At this stage of plume development, the instantaneous plume width is distributed over the entire mean-plume width (viz., $\sigma_r \approx \sigma_a$ in Fig. 2) and plume meander no longer contributes as a source of (external) concentration fluctuations at this stage of plume development. In this regime of plume development, the dispersion is expected to be similar to Brownian diffusion. This phase of development can be described

using an eddy diffusivity approximation with $\sigma_r \sim (D_t t)^{1/2}$ where $D_t \approx C_{s1} k^2/\epsilon$ is the eddy diffusivity. This approximation for the eddy diffusivity uses only the (dominant) isotropic part of the tensor diffusivity given by Eq. (13). Furthermore, the full turbulence energy is available as the relative dispersion energy in this stage of plume development, so the characteristic velocity scale for concentration fluctuations is $\Delta v = k^{1/2}$ for $\sigma_r \gg \Lambda_I$. Consequently, in this regime, the dissipation time scale is given by

$$t_d \propto \sigma_r/\Delta v = \frac{(D_t t)^{1/2}}{k^{1/2}}, \qquad \sigma_r \gg \Lambda_I. \tag{20}$$

A model for scalar dissipation that is valid in the various regimes of plume development can be obtained by blending the results of Eqs. (19) and (20) to span all scales of motion. To this purpose, the velocity scale $\Delta v(\Lambda_d)$ for concentration fluctuations is formulated as follows:

$$\Delta v(\Lambda_d) = k^{1/2} \min\left(\left(\frac{\Lambda_d}{\Lambda_I} \right)^{1/3}, 1 \right), \qquad \Lambda_d \geq \sigma_0. \tag{21}$$

Here, Λ_d is a dissipation length scale for concentration fluctuations which, for $\sigma_r \ll \Lambda_I$ was identified with l_e in Eq. (19) with a temporal (or, equivalently, spatial) development given by Eq. (18), and for $\sigma_r \gg \Lambda_I$ was identified with $(D_t t)^{1/2}$ in Eq. (20). These two estimates for Λ_d (valid in different regimes of plume development) can be combined, using a blending function that is similar to one proposed by Cassiani et al. (2005) for use with a micromixing time scale, to give the following generalized formulation for Λ_d:

$$\Lambda_d^2 = \frac{l_e^2}{1 + (l_e^2 - \sigma_0^2)/(\sigma_0^2 + c_1 D_t t)}, \tag{22}$$

where l_e is determined in accordance to Eq. (18) and c_1 is a closure constant. This blending (interpolation) formula satisfies the prescribed features of Λ_d at small and large travel times: namely, (1) $\Lambda_d \to \sigma_0$ as $t \to 0^+$; (2) for travel times such that $l_e \ll (c_1 D_t t)^{1/2}$ (inertial subrange time scales), $\Lambda_d \approx l_e$ corresponding to the phase of plume development where meandering is important; and, (3) for large travel times such that $l_e \gg (c_1 D_t t)^{1/2}$, $\Lambda_d \approx (c_1 D_t t)^{1/2}$ corresponding to the turbulent diffusive phase of plume development where the dispersion can be described as a Brownian diffusion. Given Eqs. (21) and (22), the scalar dissipation ϵ_c is modeled as

$$\epsilon_c = c_2 \frac{\Delta v(\Lambda_d)}{\Lambda_d} \overline{c'^2}, \tag{23}$$

where c_2 is a closure constant.

The closure constants in Eqs. (22) and (23) assume the following values: $c_1 = 0.37$ and $c_2 = 1.1$. These closure constants were chosen to provide reasonable agreement with data for a plume dispersing in an idealized obstacle array (which will be described later). More specifically, these closure constants were chosen to be consistent with the decay of the plume centerline concentration variance with increasing distance from the source. Furthermore, it has been found that the values of these closure constants only determine the level and rate of decay of the concentration variance with downwind distance along the plume centerline. They do not mould the complex shape of the profiles of concentration variance in the crosswind direction.

2.4 Concentration probability density function component

The first two components of the model (described above) allow the prediction of the mean concentration C and concentration variance $\overline{c'^2}$ for a plume dispersing in an urban area. However, these two concentration statistics do not provide an adequate description of the plume concentration fluctuation statistics, without also specifying the form of the concentration PDF. To this purpose, we propose a model for the one-point concentration PDF $f(\chi; \mathbf{x})$ at a receptor point $\mathbf{x} \equiv (x, y, z)$:

$$f(\chi; \mathbf{x})\, d\chi \equiv \Pr\{\chi \leq c(\mathbf{x}) < \chi + d\chi\}, \tag{24}$$

where $\Pr\{\cdot\}$ denotes the "probability that", c is the instantaneous concentration, and χ is a sample space values for c.

Yee and Chan (1997) proposed a left-shifted clipped-gamma distribution for the concentration PDF for plumes dispersing in an unobstructed (open) terrain. In this model, the concentration PDF assumes the following form:

$$\begin{aligned} f(\chi; \mathbf{x}) \quad &= \quad \left(\frac{\chi + \lambda}{s} \right)^{k^*-1} \frac{\exp\big(-(\chi+\lambda)/s\big)}{s\Gamma(k^*)} \\ &\quad + (1-\gamma)\delta(\chi), \end{aligned} \tag{25}$$

with $k^* = k^*(\mathbf{x}) > 0$, $s = s(\mathbf{x}) > 0$, $\lambda = \lambda(\mathbf{x}) \geq 0$, $\gamma = \gamma(\mathbf{x}) \in [0, 1]$. Furthermore, $\Gamma(x)$ is the gamma function, $\delta(x)$ is the Dirac delta function and the range for χ is $0 \leq \chi < \infty$. The concentration PDF in Eq. (25) is composed of a mixed fluid part (first term on right-hand side of equation) that results from in-plume mixing of eddies that contain the scalar contaminant, and an unmixed ambient fluid part (second term on right-hand side of equation) that is produced by plume meandering producing intermittent periods of zero concentration for a fraction of time $(1 - \gamma)$. Alternatively, $\gamma \equiv \Pr\{c(\mathbf{x}) > 0\}$ is the intermittency factor that determines the probability of observing a non-zero instantaneous concentration c at $\mathbf{x}$.

The concentration PDF in Eq. (25) is completely determined by four parameters: namely, γ, k^*, s and λ. However, only three of these parameters are independent, owing to the fact that the intermittency factor γ is determined uniquely as the area remaining under the gamma PDF curve for $\chi > 0$ after a left-shift of χ by the amount $\lambda \geq 0$; hence,

$$\begin{aligned} \gamma \equiv \gamma(k^*, s, \lambda) \quad &= \quad \int_\lambda^\infty \left(\frac{\chi}{s} \right)^{k^*-1} \frac{\exp(-\chi/s)}{s\Gamma(k^*)}\, d\chi \\ &= \quad \int_0^\infty \left(\frac{\chi + \lambda}{s} \right)^{k^*-1} \frac{\exp(-(\chi+\lambda)/s)}{s\Gamma(k^*)}\, d\chi \\ &= \quad \frac{\Gamma(k^*; \lambda/s)}{\Gamma(k^*)}, \end{aligned} \tag{26}$$

where $\Gamma(\nu; x)$ denotes the complementary incomplete gamma function.

To use the clipped-gamma distribution for our current application, we need a particular form that is completely specified by two parameters, whose values can be determined using the predicted values for the mean concentration and concentration variance. To this objective, Yee and Chan (1997) imposed an additional constraint on the form of the clipped-gamma distribution; namely, they used a comprehensive data set of measurements of plume concentration fluctuations in open terrain to formulate the following simple relationship between

the normalized mean-square concentration and the plume intermittency:

$$\gamma = \min\left(1, \frac{3}{\overline{(c/C)^2}}\right). \tag{27}$$

The model concentration PDF parameters k^*, s and λ in Eq. (25) can be obtained by application of the method of moments applied to the normalized concentration c/C. Using the method based on moments for c/C, the identification of the parameters k^*, s and λ requires the solution of the following system of transcendental equations:

$$\frac{1}{s} = \left(-\frac{\lambda}{s} + k^*\right)\gamma + \frac{1}{\Gamma(k^*)}\left(\frac{\lambda}{s}\right)^{k^*} e^{-\lambda/s}; \tag{28}$$

$$\overline{\left(\frac{c}{C}\right)^2} = \frac{\left((\lambda/s)\gamma + (-\lambda/s + k^* + 1)/s\right)}{\left[(-\lambda/s + k^*)\gamma + (\lambda/s)^{k^*} e^{-\lambda/s}/\Gamma(k^*)\right]^2}; \tag{29}$$

and

$$\gamma = \min\left(1, 3\Big/\overline{\left(\frac{c}{C}\right)^2}\right) = \frac{\Gamma(k^*; \lambda/s)}{\Gamma(k^*)}. \tag{30}$$

Consequently, for a specified value of $\overline{(c/C)^2}$, Eqs. (29) and (30) need to be solved for k^* and λ/s. Next, these values can then be subsequently substituted into Eq. (28) to obtain s, after which the value of λ can be obtained. Note that even though the clipped-gamma distribution involves three parameters (s, k^* and λ), only k^* and λ/s are independent because s can be expressed explicitly in terms of k^* and λ/s by virtue of Eq. (28). In consequence, the clipped-gamma distribution is actually only a two-parameter distribution.

The solution of these equations for k^*, s and λ as a function of $\overline{(c/C)^2}$ is exhibited in Fig. 3. Note that k^* is a monotonically decreasing function of normalized mean-squared concentration, whereas s and λ are both monotonically increasing functions of the normalized mean-squared concentration. The parameters shown in Fig. 3 define the clipped-gamma probability law for the normalized concentration, χ/C [viz., determine the functional form for the clipped-gamma distribution $f(\chi/C)$].

The clipped-gamma PDF of Eq. (25) gives the following explicit form for the cumulative distribution function (CDF) for the concentration (at the receptor point $\mathbf{x}$):

$$\begin{aligned} F(\chi;\mathbf{x}) \equiv \Pr\{c(\mathbf{x}) \le \chi\} &= \int_{0^-}^{\chi} f(\chi';\mathbf{x})\, d\chi' \\ &= 1 - \frac{\Gamma(k^*; (\chi+\lambda)/s)}{\Gamma(k^*)}. \end{aligned} \tag{31}$$

The complement of the concentration CDF [or, exceedance distribution function (EDF) for concentration] is simply $\big(1 - F(\chi;\mathbf{x})\big) \equiv \Pr\{c(\mathbf{x}) > \chi\}$.

3. APPLICATION TO IDEALIZED OBSTACLE ARRAY

In this section, we evaluate the predictive accuracy of the probabilistic model for urban dispersion by presenting the results of a detailed comparison of the flow and turbulent dispersion between a comprehensive water-channel experiment and the model predictions.

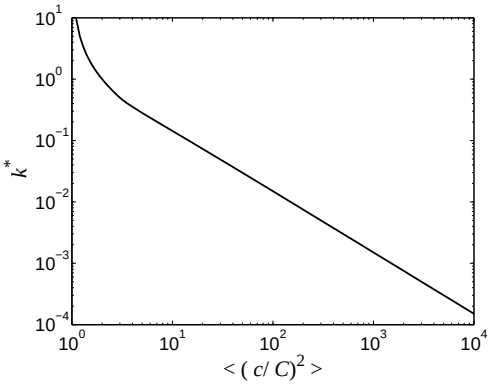

(a) Clipped-gamma parameter k^*

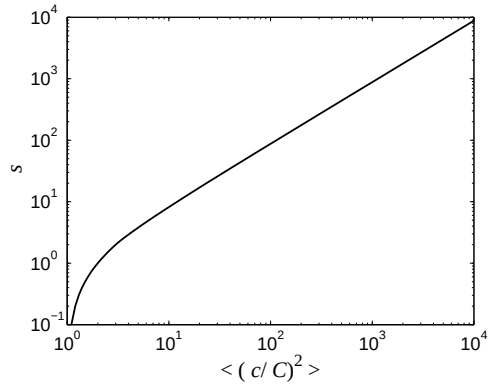

(b) Clipped-gamma parameter s

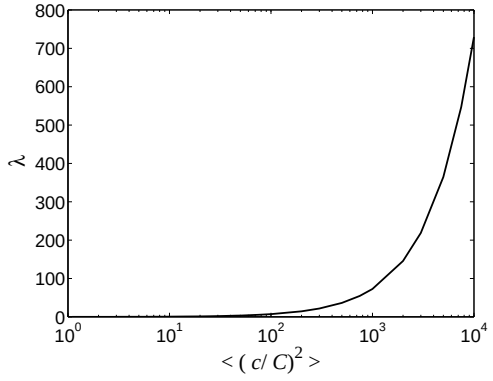

(c) Clipped-gamma parameter λ

Figure 3: Dependence of the parameters (k^*, s, and λ) of a clipped-gamma distribution on the normalized mean-square concentration $\langle (c/C)^2 \rangle \equiv \overline{(c/C)^2}$, where C is the mean concentration.

3.1 Water-channel experiment

The water-channel experiment is fully described in Hilderman and Chong (2007), and only the important details of the experiment will be presented here. The experiment, which was commissioned by Defence R&D Canada – Suffield, was conducted in the boundary-layer water channel at Coanda Research

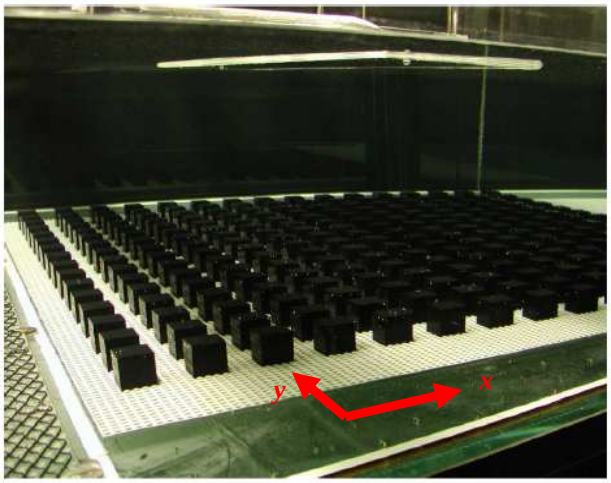

Figure 4: A photograph showing the geometry of the regular and aligned array of cubes placed in a boundary-layer water channel at Coanda Research & Development Corporation (Burnaby, British Columbia, Canada). The Cartesian coordinate system used is also shown. Here, x is in the streamwise direction and y is in the spanwise direction.

& Development Corporation (Burnaby, British Columbia, Canada). The water channel had a working section of 10 m length, 1.5 m width and 0.9 m height.

The water-channel experiment simulated a neutrally-stratified atmospheric boundary-layer flow over a regular array of three-dimensional (3-D) obstacles. The 3-D obstacle array is shown in Fig. 4. The array consists of sharp-edged cubes with a characteristic dimension $L = W = H = 31.75$ mm, where L, W and H are the length, width and height of the obstacles. A total of 256 cubes was placed in an aligned array consisting of 16 rows of 16 cubes. The array filled the entire spanwise dimension (width) of the water channel. The streamwise and spanwise face-to-face spacings between cubes was H, giving frontal and plan area indices (λ_f and λ_p, respectively) of 0.25.

The building array was immersed in a simulated neutral atmospheric boundary layer that was created in the water channel using the combination of a "turbulence" grid made of square bars 19 mm × 19 mm placed at the start of the channel inlet and a sawtooth fence, with a base width equal to that of the channel and a height of 70 mm, placed 200 mm downstream of the square bar array. The boundary-layer thickness, δ, taken to be the height where the mean wind speed reached 99% of the free-stream value, was found to be 275 mm. At this point, the mean wind speed $\overline{u}_\delta$ was 0.375 m s^{-1}. The friction velocity u_* determined from measurements of the shear stress in the constant stress layer near the surface of the upstream fetch was 0.0255 m s^{-1}, giving $u_*/\overline{u}_\delta = 0.068$ for the water-channel simulations. A least-squares fit of the usual log-law profile for the mean wind speed in a regular rough-wall boundary layer, $\overline{u}/u_* = k_v \log\big[(z-d)/z_0\big]$, where z_0 is the roughness length, d is the zero-plane displacement, and $k_v \approx 0.4$ is von Kármán's constant gave the following results: $z_0 = 0.35 \pm 0.05$ mm, assuming a zero-plane displacement d of 2.8 mm (using the common rule of thumb that d should be approximately 70% of the height of the roughness elements). The reference Reynolds

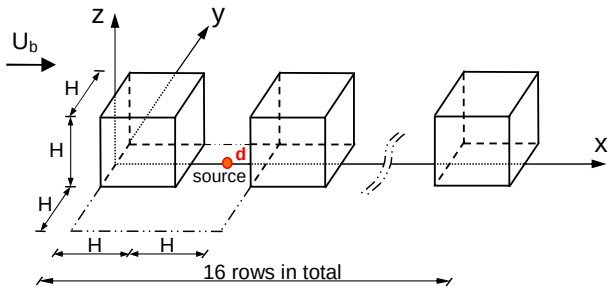

Figure 5: Geometry of the regular and aligned array of cubes in the water channel depicting the eighth column of the obstacles. The location of the ground-level source is marked by d.

number of the flow was approximately $Re_H = 12,005$ (based on H and the free-stream velocity $U_b = 0.38$ m s^{-1}).

Measurements of the velocity components were made using a 4-beam, 2-component fibre-optic laser Doppler velocimeter (LDV). The velocity time series were sampled for 500 s. This sampling time was sufficiently long to give statistically converged estimates for the various velocity statistics. For the water-channel simulations of dispersion in the obstacle array, a ground-level point source consisting of a vertical stainless steel tube (2.8 mm I.D. and 3.1 mm O.D.) was used, with the outlet of the tube placed just above the wire mesh that served as the ground roughness elements. The source emitted a sodium fluorescein dye tracer at a constant flow rate of 12×10^{-3} l min^{-1} with low discharge momentum (weak vertical jet). The source was located between the first and second rows of obstacles in the spanwise-oriented street canyon at a position lying at the intersection of the first row and eighth column of obstacles (where the rows are numbered in increasing order in the streamwise direction from the leading (windward) edge of the array and the columns are numbered in increasing order in the spanwise direction from the right-hand side of the array when looking in the flow direction – see Fig. 4). This source location will be referred to as location d as shown in Fig. 5. The instantaneous concentration field in the dispersing dye plume was measured using the laser-induced fluorescence (LIF) technique.

3.2 Velocity statistics

For the simulations of the flow and dispersion in the obstacle array, the model domain used spanned $-15 \le x/H \le 46$ with the windward face of the first row of cubes placed at $x/H = 0$. The spanwise extent of the domain was $18H$ (spanning 9 columns of cubes in the spanwise direction with $-9 \le y/H \le 9$) and the domain height was $11H$ ($0 \le z/H \le 11$), where z is the vertical coordinate direction measured from ground level. The vertical x-z center plane at $y/H = 0$ contained the ground-level source at location d (see Fig. 5). In this coordinate system, the source at d is located at $\mathbf{x}_s/H \equiv (x_s, y_s, z_s)/H = (1.5, 0, 0)$.

The model domain was discretized with a non-uniform grid of 245×149×48 control volumes (in the streamwise, spanwise and vertical directions, respectively). The grid lines were preferentially concentrated near the solid surfaces (e.g., ground, walls, rooftops) where the flow property gradients are expected to be greatest, with the spacing between the grid lines gently

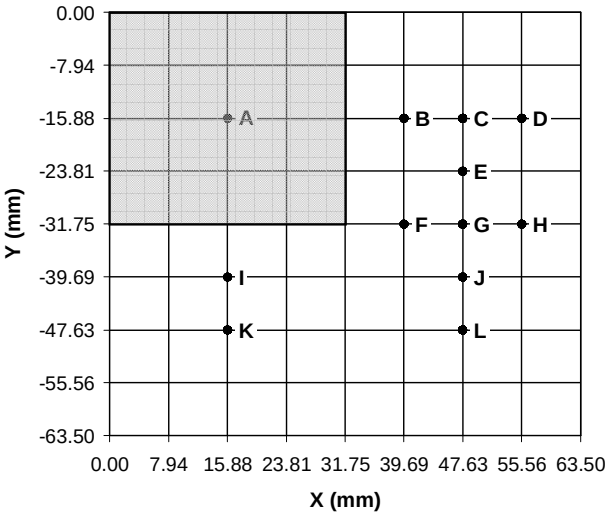

Figure 6: Sampling locations for velocity measurements in a unit cell of the cubic array. Each unit cell of the array was $2H \times 2H$, with $H = 31.75$ mm.

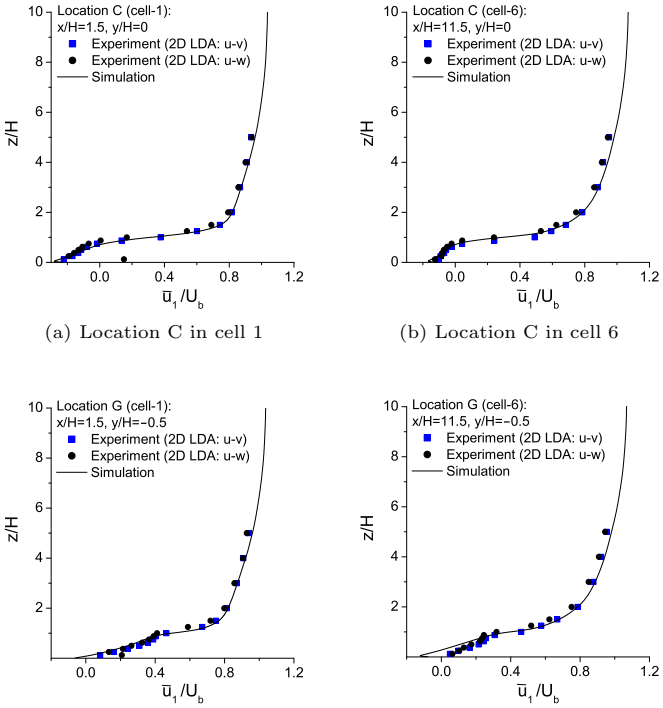

(a) Location C in cell 1

(b) Location C in cell 6

(c) Location G in cell 1

(d) Location G in cell 6

Figure 7: Comparison of measured and predicted vertical profiles of mean streamwise velocity, $\bar{u}_1 \equiv \bar{u}$, (normalized by U_b) at locations C and G in cells 1 and 6. Two different configurations of the LDV have been used to measure $\bar{u}$ (namely, the u-v and u-w configurations).

stretched with increasing distance from the solid surfaces in the spanwise and vertical directions. The grid lines were uniformly spaced in the streamwise direction, except that the grid mesh was refined in the street canyon between the first and second rows of obstacles in order to resolve the diameter of the tracer source used in the water-channel experiments.

Detailed measurements of vertical velocity profiles were made at 12 locations in two unit cells of the cubic array. The two unit cells were taken at two streamwise locations along the eighth column of cubes (near the centerline of the array). In the aligned array of cubes shown in Fig. 4, a unit cell of the array occupies a plan area of $2H \times 2H$ in the x-y plane as shown in Fig. 6. In this figure, the 12 locations for the measurements of the velocity profiles are labelled A through K. Note that the cubical obstacle occupies the upper-left quadrant of the unit cell (with location A situated at the center of this obstacle). The location of the cubical obstacle is marked by the shaded region shown in Fig. 6. Measurements of vertical profiles of the velocity were made in the first (cell 1) and sixth (cell 6) cells in the streamwise direction along the eighth column of cubes in the array.

Figure 7 compares model predicted vertical profiles of the mean streamwise velocity $\bar{u}$ (normalized by the free-stream velocity U_b) at two locations C and G in cells 1 and 6. The mean streamwise velocity profiles corresponding to locations C and G in cell 1 are located in the adjustment zone, where the undisturbed upstream flow is adjusting to the presence of the urban canopy. In contrast, the mean streamwise velocity profiles corresponding to locations C and G in cell 6 are located in the equilibrium zone, where the mean velocity appears to have reached streamwise equilibrium (viz., the mean streamwise velocity is fully developed). At all these locations, it is seen that the mean streamwise velocity is well predicted by the model. In particular, a very strong shear layer forms at the top of the urban canopy, whose signature is revealed by the inflection point in $\bar{u}(z)$ at or near the obstacle height H. Note that the large values of mean shear $\partial\bar{u}/\partial z$ just above the building height are predicted well by the model. Furthermore, at location C, the magnitude of the reverse velocity in the spanwise-oriented street canyon is correctly reproduced by the model predictions.

Figure 8 presents vertical profiles of turbulence kinetic energy, k, at the same locations as the mean streamwise velocity profiles displayed in Fig. 7. The model predictions shown here were obtained with the standard k-ϵ model with $C_{\epsilon_0} = 1$ and the modified k-ϵ model with $C_{\epsilon_0} = 0.7$.[5] Generally speaking, the turbulence energy levels in the roughness sublayer ($z/H < 2$) are under-predicted by the standard k-ϵ model. The modified k-ϵ model improves the prediction of the turbulence energy levels for $z/H < 2$. In particular, note that the observed large peak in TKE at location C in cell 1 (which is just above the first building rooftop) is well predicted using the modified k-ϵ model, whereas it is significantly under-predicted (by about a factor of two) using the standard k-ϵ model. Furthermore, the position and magnitude of the prominent nose in the k-profile at location C in cell 6 (which lies just above the street canyon top in the equilibrium zone) is largely reproduced by the modified k-ϵ model, but predicted less well by the standard k-ϵ model. The peak value of k at location C

[5]It should be noted that the predictions of the mean streamwise velocity obtained using the standard and modified k-ϵ models were virtually identical. Only the predictions of turbulence energy levels differed between the two models.

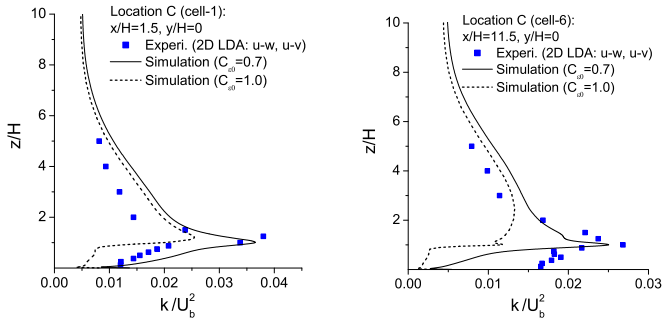

(a) Location C in cell 1

(b) Location C in cell 6

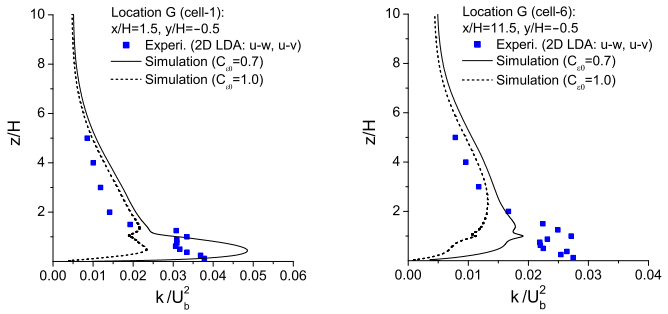

(c) Location G in cell 1

(d) Location G in cell 6

Figure 8: Comparison of measured and predicted vertical profiles of turbulence kinetic energy, k, (normalized by U_b^2) at locations C and G in cells 1 and 6 (for $C_{\epsilon_0} = 1$ and 0.7).

(which occurs at or near the canopy top at $z/H \approx 1$) decreases monotonically in the streamwise direction from the first street canyon (cell 1) and reaches a near constant value at the sixth street canyon (cell 6). This feature in the behaviour of the TKE is correctly captured by the modified k-ϵ model.

3.3 Concentration statistics

Figure 9 displays predictions for crosswind profiles of the mean concentration C (normalized by the source concentration C_s) at half-canopy height ($z/H = 0.5$) at five alongwind locations $(x - x_s)/H$. These predictions were obtained using the wind statistics derived from the RANS approach with a standard k-ϵ turbulence closure model. The corresponding experimental measurements (open circles) are also shown in the figure for comparison. In general, the predictions for the mean concentration show good agreement with the measurements at all the locations, although they are seen to over-predict slightly the mean-plume centerline concentration (at $y/H = 0$), at the farthest available x-station. Furthermore, the peak mean concentration is over-predicted by as much as about 20% at the farthest downwind station. Note that the model under-predicts the crosswind spread of the plume at alongwind locations further from the source (i.e., for $(x - x_s)/H \gtrsim 6$), which is consistent with the slight over-prediction of the mean concentration at these locations. Nevertheless, it can be inferred from the results of Fig. 9 that the horizontal spread rate of the mean plume and the rate of decay of the mean-plume centerline concentration, as a function of downwind distance from the source, is predicted quite well by the model.

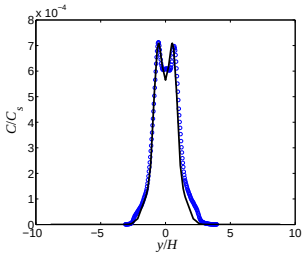

(a) $(x - x_s)/H = 2$

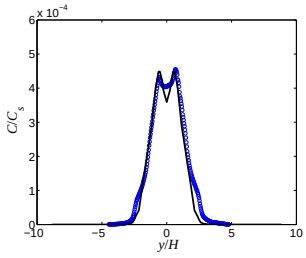

(b) $(x - x_s)/H = 4$

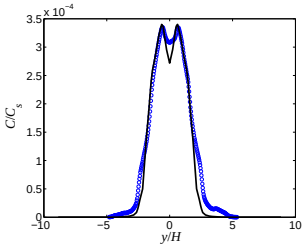

(c) $(x - x_s)/H = 6$

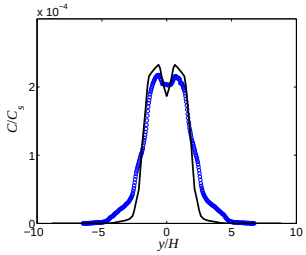

(d) $(x - x_s)/H = 10$

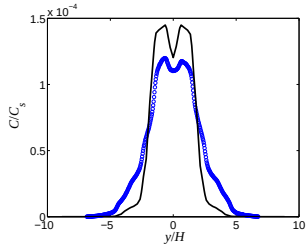

(e) $(x - x_s)/H = 16$

Figure 9: Crosswind profile of the normalized mean concentration, C/C_s, measured at various alongwind positions at half-canopy height ($z/H = 0.5$). The plot also includes a model prediction for the normalized mean concentration (solid line). Here, C_s is the source concentration.

Crosswind profiles of the concentration standard deviation, $\sigma_c \equiv \overline{(c'^2)}^{1/2}$, normalized by the source concentration C_s, are exhibited in Fig. 10 at the same alongwind locations as shown in Fig. 9. The model predictions (solid line) for σ_c are in good conformance with the experimental data (open circles) over the available downstream range. The lateral cross-sections of σ_c are similar to the C-profiles, except that they are broader and the ratio of the peak value to the centerline value of σ_c is larger. The concentration standard deviation exhibits a distinctive bimodal structure with a local minimum at the centerline. These general features of σ_c are captured adequately by the model, although the crosswind dispersion of the concentration standard deviation profiles are under-predicted by the model. The presence of off-centerline peaks in the crosswind profiles for the concentration standard deviation (or, equivalently, the concentration variance) illustrate the role of production in molding the shape of σ_c. In particular, the maximum in σ_c (or, equivalently, $\overline{c'^2}$) occurs roughly at the inflection point in the corresponding crosswind C-profile, which

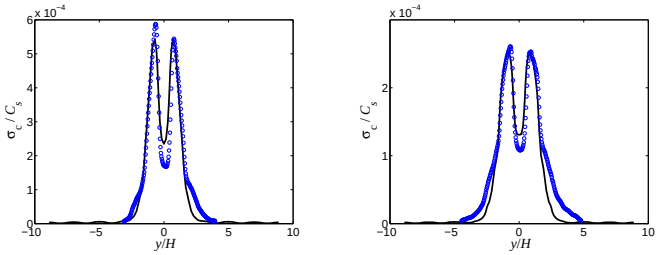

(a) $(x - x_s)/H = 2$

(b) $(x - x_s)/H = 4$

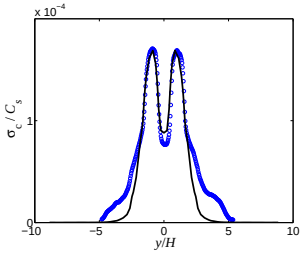

(c) $(x - x_s)/H = 6$

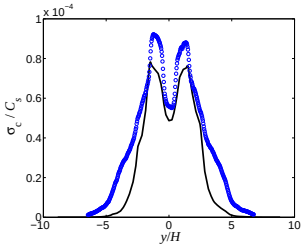

(d) $(x - x_s)/H = 10$

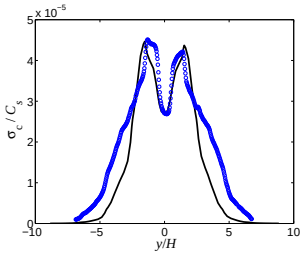

(e) $(x - x_s)/H = 16$

Figure 10: Crosswind profile of the normalized concentration standard deviation, σ_c/C_s, measured at various alongwind positions at half-canopy height ($z/H = 0.5$). The plot also includes a model prediction for the normalized concentration standard deviation (solid line). Here, $\sigma_c \equiv (\overline{c'^2})^{1/2}$ and C_s is the source concentration.

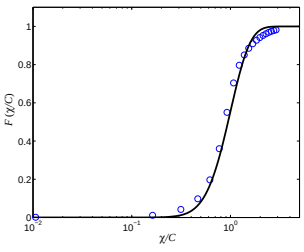

(a) $(x - x_s)/H = 2$

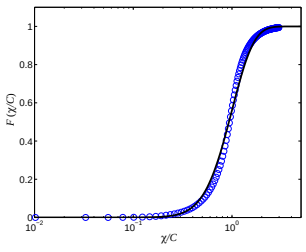

(b) $(x - x_s)/H = 4$

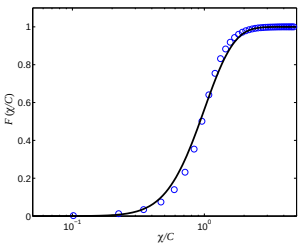

(c) $(x - x_s)/H = 6$

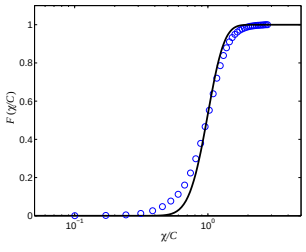

(d) $(x - x_s)/H = 10$

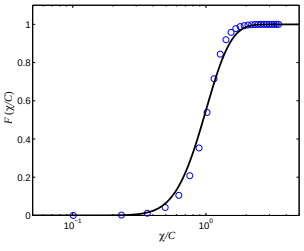

(e) $(x - x_s)/H = 16$

Figure 11: Cumulative distribution function (CDF), $F(\chi/C)$, of the normalized concentration measured at various alongwind positions from the source along the mean-plume centerline ($y/\sigma_y = 0$) and at half-canopy height ($z/H = 0.5$). The plot also includes a prediction for the concentration CDF provided by the clipped-gamma model (solid line), which was generated using the predicted normalized mean-square concentration at each plume location.

is the position (approximately or better) of maximum production ($\equiv -\overline{u_i' c'} \partial C/\partial x_i$) of $\overline{c'^2}$ in a lateral cross-section.

3.4 Concentration PDF

Given predictions of C and $\overline{c'^2}$, the prediction of probability of exceedances of critical concentration levels can be obtained using a pre-specified form of the concentration PDF. Earlier, we suggested the application of the clipped-gamma PDF for the concentration since the parameters for this PDF are uniquely defined given the information embodied in C and $\overline{c'^2}$. To this end, we compare the modeled and measured cumulative and exceedance probability distributions.

Figure 11 exhibits comparisons of the predicted and observed evolution of the CDF of χ/C along the mean-plume centerline ($y/\sigma_y = 0$, where σ_y is the mean-plume crosswind dispersion) at half-canopy height ($z/H = 0.5$). Concentration CDFs at five different downwind distances from the source, spanning the range $2 \leq (x - x_s)/H \leq 16$, are displayed in Fig. 11. The model predictions for the clipped-gamma concentration CDF were obtained by using the predicted values of C and $\overline{c'^2}$ at these locations to determine the mean-square concentration $\overline{(c/C)^2} \equiv \overline{c'^2}/C^2 + 1$, which is then used to determine the parameters k^*, s and λ for the model distribution (see Fig. 3). Generally, it can be seen that the clipped-gamma distribution is in good conformance with the measured concentration CDF. This suggests that the dynamics associated with the evolution of the fluctuating plume in the alongwind direction are being described correctly by the model.

Because it is the prediction of the likelihood of extreme events that is important in the hazard assessment of toxic gas releases, it is important to examine the upper tail of the concentration distribution. To that purpose, we exhibit in Fig. 12 the exceedance distribution functions, $1 - F(\chi/C)$, for the same plume locations shown in Fig. 11 for dispersion in the array of cubes. The exceedance distribution functions have been plotted on a logarithmic scale in order to emphasize the upper tails. Figure 12 indicates that the clipped-gamma dis-

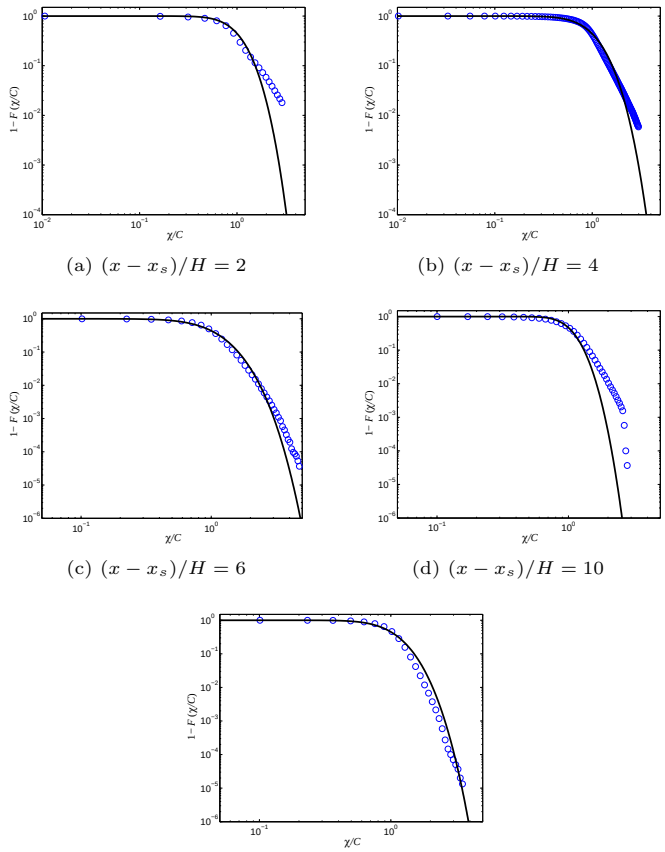

(a) $(x - x_s)/H = 2$ (b) $(x - x_s)/H = 4$

(c) $(x - x_s)/H = 6$ (d) $(x - x_s)/H = 10$

(e) $(x - x_s)/H = 16$

Figure 12: Exceedance distribution function (EDF), $1 - F(\chi/C)$, of the normalized concentration measured at various alongwind positions from the source along the mean-plume centerline ($y/\sigma_y = 0$) and at half-canopy height ($z/H = 0.5$). The plot also includes a prediction for the concentration EDF provided by the clipped-gamma model (solid line), which was generated using the predicted normalized mean-square concentration at each plume location.

tribution predicts generally the upper tail very well (except perhaps at $(x - x_s)/H = 10$ where the model concentration EDF is seen under-predict the probability of occurrence of large concentrations).

4. CONCLUSIONS

The formulation of a probabilistic model for prediction of the statistical characteristics of concentration fluctuations in pollutant plumes dispersing in an urban area is presented. This model has been derived with an emphasis towards simplicity and robustness. The principal motivation for development of such a model arises from the recognition that concentration fluctuations are critical for the proper assessment of flammable and toxic gases and from increased concerns about releases of these noxious substances in (built-up) urban areas where the population is greatest. The probabilistic model developed here allows actual or potential hazards resulting from the release of flammable, toxic, or malodourous substances to be quantified by probabilities (e.g., the probability that the concentration of a toxic material exceeds a critical intoxication level, or the probability that a flammable gas with given lower and upper flammability limits is ignitable).

A knowledge of C and $\overline{c'^2}$ for the concentration probability law does not allow one in general to determine the probability law (viz., it may require a knowledge of more than simply the first two moments of concentration to allow the determination of the probability law for concentration). In view of this, it is perhaps surprising that using only the two lowest-order concentration moments, in conjunction with the assumption that the concentration probability law has a clipped-gamma form, allowed very good predictions to be obtained for the concentration PDF for the example used in this paper. These good predictions might be extremely fortuitous. Fortunately, it turns out that this is not the case.

Some recent work (Yee, 2008a; Yee, 2008b) has shown that plume concentration data measured in both open-terrain and built-up environments exhibit a remarkably robust feature; namely, the observed collapse of the third- and fourth-order normalized concentration moments on the second-order normalized concentration moment. More surprising, the collapse of the various concentration moments in a built-up environment was found to be exactly the same as that observed in an unobstructed (open-terrain) environment. This remarkable collapse suggests that the concentration PDF of plumes dispersing in either a built-up or open-terrain environment can be described adequately by at most two parameters (namely, a location parameter which can be chosen to be the mean concentration and a scale parameter which can be chosen to be the root-mean-square concentration or, equivalently, the concentration standard deviation). Furthermore, the two-parameter probability law of concentration is universal, valid for dispersion in all forms of environments [e.g. arbitrary built-up (urban) environments, level unobstructed (rural) environments, etc.]. Finally, the general shape of the observed concentration probability distribution was found to be well approximated using the clipped-gamma distribution.

The implication of the work of Yee (2008a,b) is that the two-parameter clipped-gamma probability law of concentration can be used, in conjunction with predictive models for the mean concentration and concentration variance in urban plumes, to provide a prognostic probabilistic model for the assessment of hazards (toxicity, flammability, malodour), resulting from the dispersion of pollutant plumes in built-up areas. A full realization of this implication for probabilistic modeling of concentration fluctuations in plumes dispersing in an urban environment has been realized in this paper.

The probabilistic modeling scheme developed here is simple enough to provide a practical option for modeling concentration fluctuations in plumes dispersing through an urban area. Future work with the current model will involve coupling it with routine prognostic mesoscale meteorological models to provide an operational prediction of concentration fluctuations for releases of toxic materials in the urban environment and beyond. This will allow practical probabilistic assessments of risk associated with hazardous substance releases in an urban area.

5. ACKNOWLEDGMENTS

The authors wish to acknowledge support from the Chemical Biological Radiological Nuclear Research and Technology Initiative (CRTI) Program under project number CRTI-07-0196TD.

REFERENCES

Andronopoulos, S., D. Grigoriadis, A. Robins, A. Venetsanos, S. Rafailidis, and J. G. Bartzis, 2002: Three-dimensional modeling of concentration fluctuations in complicated geometry. *Environ. Fluid Mech*, **1**, 415–440.

Baik, J. J, J. J. Kim, and H. J. S. Fernando, 2003: A CFD model for simulating urban flow and dispersion. *J. Appl. Meteorol.*, **42**, 1636–1648.

Camelli, F. E., R. Lohner, and S. R. Hanna, 2005: VLES study of MUST experiment. 43rd AIAA Aerospace Sciences Meeting and Exhibit, Reno, Nevada, January 10–13.

Cassiani, M., P. Franzese, and U. Giostra, 2005: A PDF micromixing model of dispersion for atmospheric flow. Part I: development of the model, application to homogeneous turbulence and to neutral boundary layer. *Atmos. Environ.*, **39**, 1457–1469.

Coirier, W. J., D. M. Fricker, M. Furmanczyk, and S. Kim, 2005: A computational fluid dynamics approach for urban area transport and dispersion modeling. *Environ. Fluid Mech.*, **5**, 443–479.

Gailis, R. and A. Hill, 2006: A wind-tunnel simulation of plume dispersion within a large array of obstacles. *Boundary-Layer Meteorol.*, **119**, 289–338.

Hall, D. J., A. M. Spanton, R. W. Macdonald, and S. Walker, 1997: A simple model for estimating dispersion in urban areas. BRE Client Report CR 169/97, Building Research Establishment, Watford, UK.

Hilderman, T. and R. Chong, 2007: *A laboratory study of momentum and passive scalar transport and diffusion within and above a model urban canopy.* DRDC Suffield CR 2008-025, Defence R&D Canada – Suffield, Ralston, Alberta.

Hsieh, K. J., F.-S. Lien, and E. Yee, 2007: Numerical modeling of passive scalar dispersion in an urban canopy layer. *J. Wind Eng. Ind. Aerodyn.*, **95**, 1611–1636.

Kim, J. J. and J. J. Baik, 2004: A numerical study of the effects of ambient wind direction on flow and dispersion in urban street canyons using the RNG k-ϵ turbulence model. *Atmos Environ*, **38**, 3039–3048.

Klein, P., B. Leitl, M. Schatzmann, and D. Young, 2008: Concentration fluctuations in a downtown urban area – analysis of concentration data from the Joint Urban 2003 full-scale and wind-tunnel measurements. *Proceedings of 15th Joint Conference on the Applications of Air-Pollution Meteorology with the A&WMA*, New Orleans, LA, Paper AIRPOL 6.2.

Lien, F.-S. and E. Yee, 2004: Numerical modeling of the turbulent flow developing within and over a 3-D building array, Part I: a high-resolution Reynolds-averaged Navier-Stokes approach. *Boundary-Layer Meteorol.*, **112**, 427–466.

Milliez, M. and B. Carissimo, 2007: Numerical simulations of pollutant dispersion in an idealized urban area, for different meteorological conditions. *Boundary-Layer Meteorol*, **122**, 321–342.

Milliez, M. and B. Carissimo, 2008: Computational fluid dynamical modeling of concentration fluctuations in an idealized urban area. *Boundary-Layer Meteorol.*, **127**, 241–259.

Wang, B.-C., E. Yee, and F.-S. Lien, 2007: Study of turbulent passive scalar dispersion within a regular array of obstacles. *Proceedings of the 5th International Symposium on Turbulent Shear Flow Phenomena*, Munich, Germany. Friedrich, R., N. A. Adams, J. K. Eaton, J. A. C. Humphrey, N. Kasagi, and M. A. Leschziner (editors), pages 797–802.

Wang, B.-C., E. Yee, and F.-S. Lien, 2008: Numerical study of dispersing pollutant clouds in a built-up environment. *Int. J. Heat Fluid Flow*, doi:10.1016/j.ijheatfluidflow.2008.09.008, in press.

Williams, M. D, M. J. Brown, D. Boswell, B. Singh, and E. R. Pardyjak, 2004: Testing of the QUIC-PLUME model with wind-tunnel measurements for a high-rise building. Preprints. In: Fifth AMS symposium urban environment, Vancouver, BC, Amer Meteorol Soc, CDROM J5.3

Wilson, J. D., 2007: Technical description of urban microscale modeling system: Component 4 of CRTI Project 02–0093RD. J. D. Wilson and Associates, Edmonton, Alberta.

Yee, E., 2008a: The concentration probability density function with implications for probabilistic modeling of chemical warfare agent detector responses for source reconstruction. DRDC Suffield TR 2008-077, Defence R&D Canada – Suffield, Ralston, Alberta.

Yee, E., 2008b: Probability law of concentration in plumes dispersing in an urban area. *Env. Fluid Mech.*, DOI 10.1007/s10652-008-9113-4, in press.

Yee, E. and C. A. Biltoft, 2004: Concentration fluctuation measurements in a plume dispersing through a regular array of obstacles. *Boundary-Layer Meteorol.*, **111**, 363–415.

Yee, E. and R. Chan, 1997: A simple model for the probability density function of concentration fluctuations in atmospheric plumes. *Atmos. Environ.*, **31**, 991–1002.

Yee, E., R. Chan, P. R. Kosteniuk, G. M. Chandler, C. A. Biltoft, and J. F. Bowers, 1994: Incorporation of internal fluctuations in a meandering plume model of concentration fluctuations. *Boundary-Layer Meteorol.*, **67**, 11–39.

Yee, E., R. M. Gailis, A. Hill, T. Hilderman, and D. Kiel, 2006: Comparison of wind-tunnel and water-channel simulations of plume dispersion through a large array of obstacles with a scaled field experiment. *Boundary-Layer Meteorol.*, **121**, 389–432.

Yee, E., B.-C. Wang, and F.-S. Lien, 2009: Probabilistic model for concentration fluctuations in compact-source plumes in an urban environment. *Boundary-Layer Meteorol.*, **130**, 169–208.

Yee, E. and D. J. Wilson, 2000: A comparison of the detailed structure in dispersing tracer plumes measured in grid-generated turbulence with a meandering plume model incorporating internal fluctuations. *Boundary-Layer Meteorol.*, **94**, 253–296.

Yoshizawa, A., 1985: Statistical analysis of the anisotropy of scalar diffusion in turbulent shear flows. *Phys. Fluids*, **28**, 3226–3231.